Supporting Information for

Information Content in Fluorescence Correlation Spectroscopy: Binary Mixtures and Detection Volume Distortion

Jonathan D. Lam[1] Michael J. Culbertson,[1] Nathan P. Skinner,[1] Zachary J. Barton,[1] Daniel L. Burden[1,*]

Abstract: Supporting information describes: (1) the apparatus employed for measurements; (2) detection volume mapping; (3) relative molecular brightness determinations; (4) a description of the simulator; (5) the form of the raw simulator output data; and (6) the raw data table (180 data element matrix) analyzed in main body of the text.

1. Wheaton College, Chemistry Department, Wheaton, IL 60187

*Corresponding author

FCS Microscope: Briefly, a 543-nm laser beam is launched into a fiber optic (460 HP single mode, Thor Labs) which delivers light to the rear port of the microscope. Optical density filters are located prior to the launch to control the excitation intensity reaching the sample. Light exiting the fiber is reflected off a dichroic mirror (555DRLP, Omega Optical) to fill the back aperture of a water-immersion epiplan-apo objective (150x N.A.=1.25, Carl Zeiss). Photons from the sample are collected by the objective and passed back through the dichroic and a 590WB45 band pass filter (Omega Optical), through a focusing lens in the Axiotech Vario, and onto an externally mounted 150-μm pinhole. Light emerging from the pinhole is collected by a transfer lens and focused onto an avalanche photodiode (APD, SPCM-AQR-15, PerkinElmer Optoelectronics). Electrical pulses from the APD are then correlated with an ALV multi-tau correlator (ALV-6010, ALV-Laser). Sample solutions are measured by suspending a 50 μL aqueous droplet from the bottom of the objective using a laser power of 60 μW.

Mapping the Detection Volume: Full details of the procedure have been described previously.[1] Briefly, a 20 μL suspension of 175 nm diameter spheres (PS-Spec Fluospheres 540/560, Invitrogen Molecular Probes, Carlsbad, CA) is sonicated and applied to the surface of a silane-derivatized glass microscope slide (Silane-Prep slides, Sigma, St. Louis, MO). The carboxylated polystyrene beads adhere to the surface nonspecifically without detectable movement during the scan. For an excitation power of ~20 nW (532 nm), the maximum count rate produced during the scan is ~1000 counts/4 ms. Replicate trials on different beads produce a similar maximum count rate, within ~15% RSD. This ensures that single beads, rather than bead clusters, are used for creating maps. Using a relatively low excitation power effectively minimizes photobleaching, and produces profiles that faithfully represent the DV geometry. Step sizes of 30 to 40 nm are used for the X and Y directions; the Z step size ranges from 100 to 350 nm. Maps represent rectangular volumes that range in size from 1.5 x 1.5 x 5 μm to 3.5 x

3.5 x 14 μm in X, Y, and Z, respectively. One map is acquired from a well-aligned microscope (Figure 1B) using a 150X water-immersion objective and a 150-micron pinhole, which approximates the shape of a theoretical Gaussian (Figure 1A). A second map of an intentionally distorted DV (Figure 1C) is produced using two laser beams that are crossed in the object plane and a 150-micron pinhole.[1] Crossing the beams creates a region of constructive and destructive interference, yielding an overall DV shape that differs from the ideal Gaussian in an extreme manner.

After acquisition, the raw map data is interpolated, deconvoluted, and the background is subtracted, as previously described.[1] Although aligned and distorted beam profiles are acquired from a microscope, the idealized theoretical Gaussian beam profile can be generated within the simulator using the mathematical expression[1] for a 3D Gaussian.

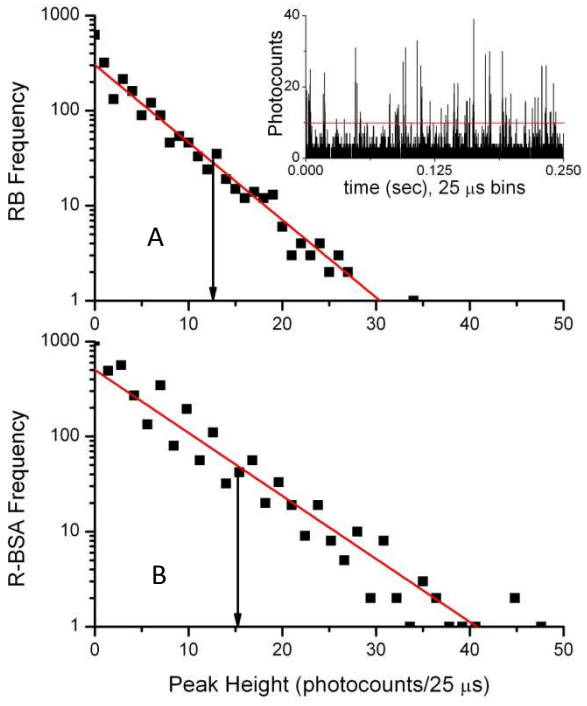

Figure S1. Peak photocount histogram analysis for relative brightness determination

Relative Brightness Determination ***(α_s):*** The brightness ratio of rhodamine-labeled bovine serum albumin (R-BSA) and rhodamine B (RB) is established by comparing fluorescent burst intensities from the real-time records of RB and R-BSA solutions. Droplets are suspended from the underside of the microscope objective and the concentration of fluorescent particles in solution is dropped to ~100 pM, which is low enough to ensure that a majority of bursts arise from only one molecule traversing the detection volume at a time. In order to

approximate an instantaneous snapshot of molecular brightness, the bin recording time (25 μs) is set considerably less than the average detection volume (DV) crossing time (~100 μs, for RB); thus, consecutive time bins record the spatial trajectory of the molecule as it moves through the DV, with the peak of the burst representing the point in time when the molecule passes nearest to the geometric center of the DV. The inset to Figure S1-A displays the photon burst record for RB. By setting a threshold (red line) to discriminate background peaks, only the largest photon bursts are selected for peak photocount analysis. The distribution of peak heights (above the threshold) are shown in panels A and B for RB and R-BSA, respectively. The peak distribution is exponential and can be fit to determine a characteristic brightness parameter, which is indicated by the arrows on the graph. This value is then added to the threshold offset (equivalent for both RB and R-BSA time recordings) and a ratio is calculated from the two sums. In this instance, the R-BSA:RB ratio is 11.7+15.1/(11.7+12.3) = 1.13.

Single-Molecule Diffusion Simulator (SMDS): The SMDS software uses Python scripts to define simulation parameters (e.g., step time, the width of time bins, overall run time, diffusion coefficients, species brightness, species mole fraction). The parallelized SMDS core algorithm is written in C and performs a random walk for particles located on a 3D lattice having periodic boundaries. A map of the DV is located at the center of this simulation space. As particles diffuse on the lattice, light is emitted relative to the particle's position within the DV. This produces a burst of photons each time a particle crosses the DV. The number of simulated photons detected in successive bin periods is assembled into a photon count vs. time record. To simulate shot noise, the final photon count for each bin is determined by randomly sampling from a Poisson distribution centered on the calculated photon sum for that bin. Each processor contributes a segment of this time record to the overall simulation time. These simulated time recordings, produced simultaneously on multiple processors, are then used to generate an autocorrelation curve.

Autocorrelation curves are produced using a distributed multi-tau autocorrelation algorithm,[2] which allows proper processing of the simulated time segments. The algorithm alleviates the need to manipulate and store a long continuous time record of photon bursts. Fluorescence records are correlated with a shift-register-based multi-tau correlator. Each processor computes the autocorrelation curve for its portion of the simulated fluorescence record and transfers the curve to a master computer to be combined with results from other machines. The master collates various portions of processed data and assembles the final autocorrelation curve. Output from this algorithm has been shown to closely match autocorrelation curves derived from a single, continuous stream of data.[2] Correlation curves derived from each of the DVs shown in Figure 1 appear distinct and reflect the geometrical differences between the three detection profiles (Figure S2).

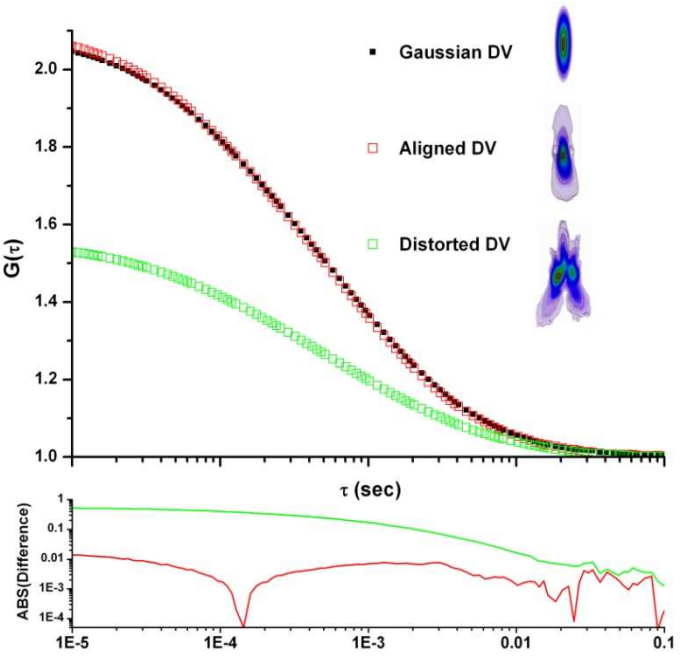

Figure S2. Different autocorrelation functions produced by variations in DV geometry

Impact of DV geometry: Figure S2 shows three autocorrelation functions (ACFs) arising from three different DVs, with all other simulation conditions remaining identical. In this case D_f = 2.9 x 10^{-6} cm^2/s, D_s = 2.9 x 10^{-7} cm^2/s (0.1x), a_f = 0.5, C_T = 0.7, α_s = 1.13. The duration for each simulation was 600s, the background count rate was 3.3 kHz, and the total count rate ranged from 160 kHz to 217 kHz, depending on the DV. Theoretical fitting functions assume a Gaussian DV geometry, which in this case gives rise to the black ACF. As can be seen, distortions in the aligned and distorted DVs produce different ACF contours. The difference arising from the

aligned DV appears to be slight (red residuals), requiring a relatively high signal-to-noise ratio in the ACF for visibility. However, the distorted DV produces a curve that differs dramatically from the Gaussian (green residuals).

Signal-to-Noise Ratio: Autocorrelation curves are fit using the Levenberg-Marquart algorithm available in Origin 8.0 Pro. The software produces a reduced chi-square parameter χ_ν^2 that indicates the quality of fit, which also reflects the signal-to-noise ratio residing in the data set. Solution and instrument parameters for the RB:R-BSA measurements are adjusted to produce χ_ν^2 values that match the values obtained from the SMDS (~10^{-6}-10^{-7}). This represents a fairly high signal-to noise ratio in the autocorrelated data, which allows the impact of DV distortion to be fully assessed and the general information limits of two-component FCS to be probed. Unless otherwise noted, simulated systems consist of 750 molecules at a concentration of 0.7 molecules/μm^3 (~1 nM) with a simulated data collection time of 600 seconds. Step times for the random walk are set to 500 ns and the background is fixed at 1.5 kHz. Total photon count rates depend upon the specific ratio of fast and slow diffusion components and range from 86-400 kHz. We also explored a limited number of scenarios consisting of lower signal-to-noise levels using photon count rates of ~10 kHz and analysis durations of 6 seconds (data not shown); however, the results show much less reproducible trends.

Simulated ACF Data Sets: Figure S3 shows autocorrelation function profiles for the different diffusion constants evaluated in this study. Small organic fluorophores possess diffusion constants of ~2.9 x 10^{-6} cm^2/s, typified by the aqueous rhodamine B samples measured on the FCS microscope. When attached to peptides or proteins, the diffusion constant shifts (typically 3-10 fold), to produce a correlation curves with a larger characteristic tau value. The curves shown here were either generated by the SMDS using the aligned DV

(Figure 1B), or were acquired directly from the FCS microscope. Panels S3-A and S3-C provide lower and upper bounds to curves acquired on the microscope. As can be seen, adjustments to

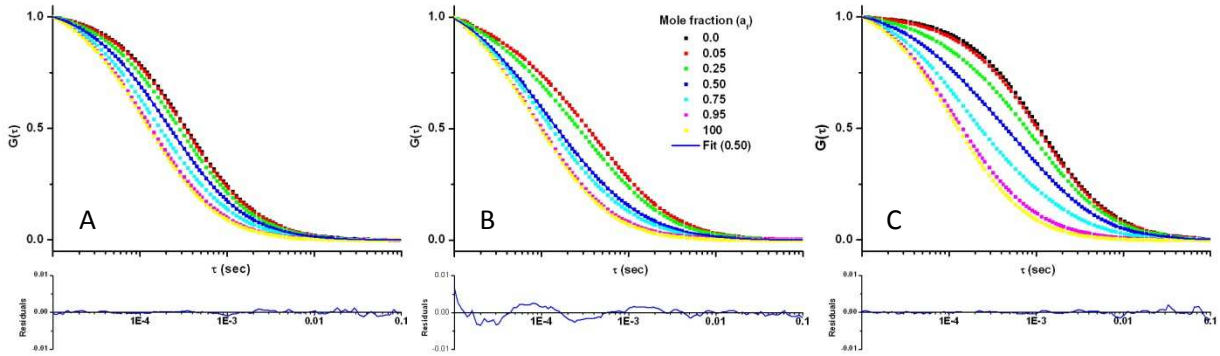

Figure S3. Autocorrelation curves for different component mixtures having a brightness ratio of 1.13. Mole fraction of the fast component (a_f) ranges from 0-100. (A) 0.33x simulation: D_f = 2.9 x 10^{-6} cm^2/s, D_s = 9.7 x $10^{-7}cm^2/s$); (B) Rhodamine B (RB), Rhodamine-labeled BSA (R-BSA) mixture; (C) 0.1x simulation: D_f = 2.9x 10^{-6} cm^2/s, D_s = 2.9 x 10^{-7} cm^2/s). The diffusion constant of R-BSA is bounded by the simulated D_s in panels A and C.

the mole fraction produce subtle distinctions in the decay profile, shifting the curves between the extremes of D_f and D_s. Fitting the a_f = 0.50 data set gives an indication of the relative signal-to-noise ratio, producing reduced chi-squared values of ~10^{-7}-10^{-6}.

Simulation Results. Because mole fraction in binary mixtures is often an unknown, it is useful to have information suggesting a range of possible error that might be incurred when these analyses are performed. Table S1 summarizes the range of average errors over all mixture compositions ($a_{f,th}$ = 0.05-0.95) for each of the parameters measured in this study (i.e., diffusion constants, mole fraction, and total concentration). Each entry in the table is calculated from an average of 3 trials at each mole fraction, with the lowest average and highest average value reported. In a majority of cases, the values defining the reported range arise from either the extreme high or extreme low mole fraction, where the signal of one of the two species is the weakest. Thus, the ranges reported in Table S1 reveal the best and worst case scenarios for analyses where species mole fraction is to be determined (e.g., dye-labeled protein solutions).

Data are organized into major categories by DV, fitting method, relative magnitude of the diffusion constant, and relative brightness. In order to quantify errors above and below the correct values for D, we use a difference factor to express the accuracy of the calculated diffusion constants (D_s and D_f), instead of percent error. The difference factor is calculated by dividing the expected value by the measured value; thus, zero percent error is represented by a difference factor of 1.0. Difference factors are not reported for D_f in the fixed category because D_f was not allowed to vary (i.e., all values are equal to 1.0). Alternatively, the convention of percent error (reported as absolute value) is used to represent errors for both a_f and C_T.

		Gaussian				Aligned				Distorted			
		Fixed D_f, Free D_s		Free D_f, Free D_s		Fixed D_f, Free D_s		Free D_f, Free D_s		Fixed D_f, Free D_s		Free D_f, Free D_s	
Relative Brightness (α_s)		0.1x	0.33x	0.1x	0.33x	0.1x	0.33x	0.1x	0.33x	0.1x	0.33x	0.1x	0.33x
		Difference Factor											
0.25	D_s	0.97-1.08	0.99-2.20	1.01-3.94	1.00-14.3	1.00-1.24	0.87-1.03	1.02-9.35	1.04-2.95	0.44-1.01	0.89-1.99	0.69-12.0	0.04-239
1	D_s	0.99-1.01	0.99-1.15	0.98-1.11	1.00-1.85	0.99-1.02	0.88-1.01	0.98-2.10	1.00-1.81	1.03-1.55	0.99-1.04	1.05-1.82	0.07-1.10
4	D_s	1.00-1.02	0.99-1.02	0.93-1.03	0.99-1.06	0.99-1.00	0.98-0.99	0.98-1.48	0.70-1.02	0.99-1.01	0.99-1.04	0.99-1.06	0.38-0.99
0.25	D_f	---	---	0.97-1.02	0.98-1.06	---	---	0.72-1.30	0.63-2.72	---	---	0.69-1.00	0.58-0.99
1	D_f	---	---	0.92-1.01	1.00-1.49	---	---	0.87-1.02	1.05-1.99	---	---	1.01-3.10	0.01-0.96
4	D_f	---	---	0.88-2.35	0.88-1.08	---	---	0.52-1.02	0.57-1.10	---	---	0.07-19.8	0.12-12000
		Percent Error											
0.25	a_f	0.23-3.59	0.56-12.8	1.58-93.9	2.80-52.4	0.15-1.79	2.15-4.87	3.06-97.5	17.3-93.5	0.09-2.66	2.09-66.7	1.28-44.7	3.60-134
1	a_f	0.13-4.95	0.02-6.50	0.18-21.2	0.62-44.4	0.00-8.12	0.54-5.03	0.50-25.9	2.43-32.6	0.64-34.9	0.2-54.8	2.07-57.6	4.51-108
4	a_f	0.06-33.8	0.10-122	0.05-543	1.06-49.8	0.09-121	0.21-343	0.06-889	0.89-694	0.07-100	0.46-100	0.40-564	3.09-73.7
0.25	C_T	0.15-1.00	0.12-8.74	0.49-26.4	0.02-16.9	6.05-7.22	4.81-7.57	0.02-17.9	2.37-12.7	30.3-31.7	29.1-38.9	27.9-71.8	2.28-41.4
1	C_T	0.07-0.61	0.21-0.46	0.06-0.70	0.20-0.47	5.54-6.48	6.20-6.39	5.52-6.38	6.15-114	32.0-32.6	31.4-32.0	31.7-32.3	31.4-32.1
4	C_T	0.08-1.16	0.02-4.20	0.17-12.9	0.52-11.1	6.22-9.65	5.62-17.4	6.41-15.4	7.62-32.0	25.7-31.2	11.6-33.5	20.6-52.1	1.81-34.1

Table S1. Range of average error (3 replicate trials) over all mixture compositions. Errors for diffusion constants are presented as a difference factor. Errors for mixture composition (a_f) and total concentration (C_T) presented as absolute percent error. Values compiled from Table S1.

As expected, the largest errors in the table occur for the distorted DV with diffusion constants of the two species differing by a factor of three, where both diffusion constants were allowed to vary (i.e., rightmost column in the table). However, it is notable that even with extremely distorted optics, reasonable accuracies can be obtained under many circumstances for each of the four measured parameters. Thus, even highly misaligned instruments can be used effectively. This underscores the utility of proper calibration, whereby a Gaussian approximation can adequately model the actual DV. Across all DVs, C_T tends to have the smallest absolute magnitude of error, as well as the smallest range of error, suggesting that the

average number density parameters ($\langle N_f \rangle$ and $\langle N_s \rangle$) are the most resilient of the fitting parameters.

The significance of the values in the table should be interpreted in tandem with the raw data from Table S2. For example, an error range of 0.50-25.9% is reported for mole fraction (a_f) with the aligned DV, two free diffusion constants, 0.1x diffusion, and equal brightness (α_s = 1). Correlating this range of errors with the data from Table S2 reveals that the largest percent error in this range arises from the smallest compositional mixture ($a_{f,th}$=0.05), where the difference between the theoretical and the measured values is only ~0.01. Thus, the upper limit of 25.9% could be misleading due to the small absolute value of a_f. However, the range of error for a_f using α_s = 4 (listed just below the 0.50-25.9% entry in Table 1) is 0.11-890%. In this case, comparison to Table S2 reveals that the largest error arises from an absolute difference in a_f of 0.44, which is more significant.

Table S2 contains the raw data set from which Table S1 is derived. All 180 parameter combinations for the 5 dimensional data are included. Values of C_T, a_f, and D_i are reported as the mean of three trials representing a total of 540 separate simulations.

Table S2

FIXED

Detection Volume Profile	Diffusion Constant Difference Factor	α_S	$a_{f,th}$	C_T	SEM	a_f	SEM	D_S (cm^2/s)	SEM
Gaussian (Fig. 1A)	0.1x	0.25	0.05	0.699	0.0036	0.0501	0.0001	2.90E-07	1.37E-09
			0.3	0.701	0.0027	0.3040	0.0022	2.81E-07	4.56E-09
			0.5	0.702	0.0009	0.5043	0.0022	2.92E-07	6.47E-09
			0.7	0.703	0.0021	0.7016	0.0055	3.14E-07	2.74E-08
			0.95	0.693	0.0031	0.9841	0.0061	2.86E-07	2.73E-08
		1	0.05	0.699	0.0013	0.0525	0.0029	2.88E-07	2.08E-09
			0.3	0.703	0.0009	0.3019	0.0575	2.89E-07	2.08E-09
			0.5	0.702	0.0010	0.5030	0.0018	2.89E-07	1.58E-09
			0.7	0.704	0.0019	0.7022	0.0001	2.92E-07	2.79E-09
			0.95	0.704	0.0009	0.9512	0.0017	2.86E-07	1.07E-08
		4	0.05	0.708	0.0113	0.0669	0.0294	2.90E-07	2.36E-09
			0.3	0.695	0.0090	0.2846	0.0215	2.93E-07	1.61E-09
			0.5	0.701	0.0027	0.4994	0.0061	2.91E-07	7.98E-10
			0.7	0.701	0.0012	0.8023	0.0989	2.91E-07	7.98E-10
			0.95	0.704	0.0008	0.9505	0.0004	2.95E-07	2.95E-09
	0.33x	0.25	0.05	0.705	0.0016	0.0503	0.0008	9.62E-07	9.72E-09
			0.3	0.703	0.0004	0.2975	0.0028	1.01E-06	1.34E-08
			0.5	0.701	0.0067	0.5045	0.0152	9.74E-07	8.06E-08
			0.7	0.723	0.0083	0.6555	0.0188	1.36E-06	3.58E-08
			0.95	0.761	0.0535	0.8285	0.1118	2.13E-06	7.09E-07
		1	0.05	0.702	0.0013	0.0532	0.0020	9.66E-07	1.99E-09
			0.3	0.701	0.0017	0.2999	0.0036	9.65E-07	8.86E-09
			0.5	0.703	0.0017	0.5007	0.0020	9.69E-07	5.55E-09
			0.7	0.703	0.0010	0.6980	0.0016	9.84E-07	1.30E-08
			0.95	0.703	0.0009	0.9455	0.0046	1.11E-06	5.42E-08
		4	0.05	0.729	0.0141	0.1108	0.0348	9.64E-07	4.60E-09
			0.3	0.707	0.0043	0.3092	0.0089	9.69E-07	8.61E-10
			0.5	0.700	0.0004	0.4924	0.0045	9.73E-07	3.25E-09
			0.7	0.704	0.0029	0.7023	0.0091	9.68E-07	7.54E-09
			0.95	0.706	0.0032	0.9491	0.0011	9.87E-07	1.91E-08
Aligned (Fig. 1B)	0.1x	0.25	0.05	0.743	0.0019	0.0497	0.0019	2.93E-07	1.50E-09
			0.3	0.742	0.0019	0.3006	0.0019	2.89E-07	6.74E-09
			0.5	0.743	0.0011	0.4992	0.0011	3.03E-07	1.25E-08
			0.7	0.750	0.0049	0.6875	0.0049	3.59E-07	2.94E-08
			0.95	0.751	0.0056	0.9391	0.0056	3.45E-07	1.34E-07
		1	0.05	0.743	0.0010	0.0541	0.0010	2.88E-07	2.89E-09
			0.3	0.739	0.0023	0.3008	0.0023	2.86E-07	1.64E-09
			0.5	0.742	0.0007	0.5017	0.0007	2.92E-07	2.26E-09
			0.7	0.743	0.0009	0.6985	0.0009	2.86E-07	2.19E-09
			0.95	0.745	0.0010	0.9500	0.0010	2.96E-07	1.75E-08
		4	0.05	0.768	0.0111	0.1107	0.0111	2.86E-07	1.64E-09
			0.3	0.756	0.0059	0.3256	0.0059	2.88E-07	8.41E-10
			0.5	0.748	0.0015	0.5170	0.0015	2.88E-07	2.52E-09
			0.7	0.745	0.0009	0.7049	0.0009	2.90E-07	1.47E-09
			0.95	0.744	0.0033	0.9508	0.0033	2.86E-07	4.66E-09
	0.33x	0.25	0.05	0.752	0.0037	0.0524	0.0018	9.45E-07	1.96E-08
			0.3	0.739	0.0018	0.3139	0.0040	9.00E-07	1.48E-08
			0.5	0.734	0.0054	0.5243	0.0116	9.17E-07	3.60E-08
			0.7	0.734	0.0080	0.7256	0.0179	8.40E-07	9.33E-08
			0.95	0.753	0.0031	0.9296	0.0071	1.00E-06	3.45E-07
		1	0.05	0.743	0.0016	0.0516	0.0072	9.76E-07	9.55E-09
			0.3	0.743	0.0003	0.3151	0.0041	9.53E-07	9.17E-09
			0.5	0.744	0.0008	0.5084	0.0026	9.57E-07	4.41E-09
			0.7	0.744	0.0012	0.7038	0.0025	9.62E-07	9.49E-09
			0.95	0.745	0.0008	0.9572	0.0016	8.53E-07	3.37E-08
		4	0.05	0.822	0.0071	0.2214	0.0141	9.65E-07	9.81E-10
			0.3	0.821	0.0020	0.4573	0.0020	9.50E-07	1.38E-09
			0.5	0.766	0.0117	0.5509	0.0241	9.64E-07	8.28E-09
			0.7	0.750	0.0009	0.7306	0.0053	9.54E-07	5.66E-09
			0.95	0.739	0.0028	0.9520	0.0010	9.49E-07	7.68E-09
Distorted (Fig. 1C)	0.1x	0.25	0.05	0.917	0.0016	0.0487	0.0003	2.93E-07	4.58E-09
			0.3	0.918	0.0005	0.3072	0.0016	2.83E-07	7.52E-09
			0.5	0.917	0.0030	0.5075	0.0056	2.64E-07	1.41E-08
			0.7	0.912	0.0071	0.7184	0.0130	2.43E-07	3.42E-08
			0.95	0.922	0.0031	0.9508	0.0048	1.28E-07	4.76E-08
		1	0.05	0.928	0.0018	0.0326	0.0009	2.98E-07	8.55E-10
			0.3	0.925	0.0018	0.2859	0.0008	3.04E-07	2.33E-09
			0.5	0.925	0.0010	0.4878	0.0012	3.08E-07	1.18E-09
			0.7	0.925	0.0012	0.6906	0.0030	3.29E-07	6.02E-09
			0.95	0.924	0.0004	0.9439	0.0035	4.48E-07	4.68E-08
		4	0.05	0.894	0.0005	0.0000	0.0000	2.87E-07	1.23E-09
			0.3	0.880	0.0118	0.2219	0.0196	2.91E-07	1.02E-09
			0.5	0.902	0.0042	0.4603	0.0065	2.94E-07	1.70E-09
			0.7	0.915	0.0040	0.6876	0.0053	2.91E-07	1.81E-09
			0.95	0.919	0.0022	0.9506	0.0002	2.89E-07	5.05E-09
	0.33x	0.25	0.05	0.915	0.0021	0.0472	0.0007	9.71E-07	7.84E-09
			0.3	0.927	0.0061	0.2808	0.0165	1.01E-06	8.00E-08
			0.5	0.972	0.0143	0.4126	0.0255	1.29E-06	1.02E-07
			0.7	0.930	0.0360	0.6854	0.0901	8.65E-07	2.23E-07
			0.95	0.904	0.0082	0.3161	0.3161	1.93E-06	9.47E-07
		1	0.05	0.924	0.0018	0.0226	0.0083	9.92E-07	1.15E-08
			0.3	0.924	0.0002	0.2748	0.0060	9.98E-07	8.17E-09
			0.5	0.921	0.0016	0.4796	0.0044	1.01E-06	1.01E-08
			0.7	0.921	0.0007	0.6815	0.0051	1.01E-06	1.06E-08
			0.95	0.920	0.0001	0.9481	0.0025	9.63E-07	4.66E-08
		4	0.05	0.898	0.0009	0.0000	0.0000	9.64E-07	1.54E-09
			0.3	0.804	0.0207	0.0684	0.0439	9.82E-07	2.44E-09
			0.5	0.781	0.0142	0.2368	0.0305	1.01E-06	4.43E-09
			0.7	0.903	0.0041	0.6550	0.0084	9.82E-07	4.87E-09
			0.95	0.934	0.0044	0.9456	0.0002	1.01E-06	9.31E-09

FREE

Detection Volume Profile	Diffusion Constant Difference Factor	α_S	$a_{f,th}$	C_T	SEM	a_f	SEM	D_S (cm^2/s)	SEM	D_F (cm^2/s)	SEM
Gaussian (Fig. 1A)	0.1x	0.25	0.05	0.697	0.0036	0.0492	0.0001	2.93E-07	2.15E-09	2.95E-06	4.19E-09
			0.3	0.704	0.0039	0.2932	0.0042	2.98E-07	9.50E-09	2.93E-06	7.57E-09
			0.5	0.714	0.0061	0.4777	0.0137	3.29E-07	1.06E-08	2.93E-06	1.29E-08
			0.7	0.745	0.0105	0.6095	0.0230	4.74E-07	6.20E-08	2.95E-06	9.16E-09
			0.95	0.885	0.1052	0.0580	0.0303	1.14E-06	7.80E-07	2.82E-06	9.51E-08
		1	0.05	0.700	0.0014	0.0606	0.0107	2.85E-07	4.68E-09	2.67E-06	6.23E-07
			0.3	0.705	0.0029	0.3050	0.0024	2.88E-07	2.80E-09	2.88E-06	2.83E-08
			0.5	0.702	0.0009	0.5024	0.0041	2.90E-07	3.67E-09	2.90E-06	2.41E-08
			0.7	0.704	0.0020	0.7013	0.0011	2.93E-07	2.90E-09	2.90E-06	7.60E-09
			0.95	0.703	0.0009	0.9462	0.0028	3.22E-07	1.92E-08	2.92E-06	5.32E-09
		4	0.05	0.790	0.0978	0.3217	0.2955	2.76E-07	1.61E-08	6.81E-06	3.43E-06
			0.3	0.668	0.0455	0.5360	0.2381	2.71E-07	3.36E-09	2.54E-06	1.51E-06
			0.5	0.697	0.0113	0.4899	0.0255	2.91E-07	2.91E-09	3.19E-06	4.56E-07
			0.7	0.699	0.0024	0.6952	0.0056	2.92E-07	1.39E-09	3.01E-06	8.41E-08
			0.95	0.706	0.0013	0.9495	0.0009	3.00E-07	6.27E-09	2.94E-06	4.03E-08
	0.33x	0.25	0.05	0.700	0.0128	0.0486	0.0054	9.73E-07	3.13E-08	2.95E-06	1.04E-07
			0.3	0.714	0.0033	0.2508	0.0190	1.12E-06	5.39E-08	2.95E-06	2.34E-08
			0.5	0.722	0.0250	0.3733	0.1364	1.27E-06	3.53E-07	3.02E-06	1.20E-07
			0.7	0.766	0.0501	0.3330	0.1682	3.62E-06	1.41E-06	3.08E-06	2.39E-07
			0.95	0.819	0.1226	0.7001	0.2675	1.39E-05	1.07E-05	2.84E-06	5.46E-08
		1	0.05	0.703	0.0004	0.0278	0.0042	9.87E-07	1.89E-09	4.31E-06	5.30E-07
			0.3	0.701	0.0018	0.2798	0.0158	9.80E-07	1.35E-08	3.04E-06	1.06E-07
			0.5	0.703	0.0017	0.5031	0.0208	9.66E-07	2.53E-08	2.89E-06	6.55E-08
			0.7	0.702	0.0009	0.6701	0.0224	1.03E-06	4.22E-08	2.97E-06	5.86E-08
			0.95	0.703	0.0009	0.7584	0.0713	1.79E-06	1.87E-07	3.13E-06	7.41E-08
		4	0.05	0.710	0.0084	0.0654	0.0225	9.70E-07	4.94E-09	3.14E-06	1.48E-06
			0.3	0.778	0.0573	0.4493	0.1206	9.58E-07	7.98E-09	2.55E-06	7.05E-07
			0.5	0.718	0.0311	0.5307	0.0728	9.67E-07	1.18E-08	2.82E-06	4.93E-07
			0.7	0.704	0.0148	0.7152	0.0488	9.60E-07	2.01E-08	2.84E-06	3.03E-07
			0.95	0.724	0.0163	0.9399	0.0075	1.03E-06	5.09E-08	3.04E-06	1.43E-07
Aligned (Fig. 1B)	0.1x	0.25	0.05	0.739	0.0021	0.0485	0.0003	2.97E-07	1.79E-09	2.97E-06	2.33E-08
			0.3	0.745	0.0026	0.2907	0.0042	3.05E-07	1.21E-08	2.93E-06	7.96E-09
			0.5	0.700	0.0659	0.3028	0.1489	1.23E-06	8.65E-07	2.10E-06	8.54E-07
			0.7	0.812	0.0260	0.4848	0.0508	5.83E-07	9.68E-08	2.97E-06	2.35E-08
			0.95	0.825	0.0906	0.0234	0.0216	2.71E-06	1.77E-07	3.77E-06	1.74E-06
		1	0.05	0.744	0.0009	0.0629	0.0108	2.84E-07	5.63E-09	2.54E-06	4.38E-07
			0.3	0.739	0.0022	0.2985	0.0023	2.88E-07	2.89E-09	2.94E-06	3.14E-08
			0.5	0.742	0.0008	0.4970	0.0046	2.95E-07	4.67E-09	2.95E-06	4.17E-08
			0.7	0.743	0.0009	0.6897	0.0008	2.96E-07	3.16E-09	2.96E-06	4.71E-09
			0.95	0.745	0.0007	0.9406	0.0019	6.10E-07	2.76E-07	2.97E-06	3.26E-08
		4	0.05	0.808	0.0601	0.4946	0.2703	4.29E-07	1.44E-07	1.51E-06	1.06E-06
			0.3	0.774	0.0223	0.3603	0.0417	2.88E-07	2.52E-09	2.59E-06	6.30E-07
			0.5	0.760	0.0019	0.5411	0.0096	2.85E-07	2.48E-09	2.52E-06	6.96E-08
			0.7	0.745	0.0033	0.7052	0.0101	2.90E-07	2.94E-09	2.91E-06	1.51E-07
			0.95	0.747	0.0058	0.9494	0.0015	2.92E-07	1.02E-08	2.96E-06	5.57E-08
	0.33x	0.25	0.05	0.717	0.0254	0.0414	0.0094	1.01E-06	6.44E-08	3.23E-06	2.07E-07
			0.3	0.626	0.0630	0.1018	0.0821	2.45E-06	7.07E-07	1.83E-06	5.66E-07
			0.5	0.730	0.0634	0.0691	0.0367	2.36E-06	4.22E-07	2.85E-06	6.20E-07
			0.7	0.789	0.0740	0.0452	0.0212	2.86E-06	3.95E-07	4.17E-06	1.28E-06
			0.95	0.736	0.0107	0.3353	0.3323	1.88E-06	9.23E-07	7.88E-06	3.89E-06
		1	0.05	0.743	0.0014	0.0353	0.0163	9.87E-07	1.60E-08	5.78E-06	1.94E-06
			0.3	0.743	0.0004	0.2927	0.0189	9.70E-07	1.94E-08	3.05E-06	9.70E-08
			0.5	0.744	0.0009	0.4662	0.0315	1.00E-06	3.36E-08	3.08E-06	1.15E-07
			0.7	1.500	0.7568	0.4716	0.1545	1.07E-06	2.99E-08	3.08E-06	4.06E-08
			0.95	0.744	0.0007	0.7512	0.0416	1.75E-06	8.90E-08	3.21E-06	5.03E-08
		4	0.05	0.924	0.0689	0.3972	0.1220	9.54E-07	7.98E-09	2.28E-06	4.49E-03
			0.3	0.814	0.0945	0.7970	0.1391	6.80E-07	2.25E-07	1.65E-06	4.23E-07
			0.5	0.782	0.0489	0.5488	0.1121	9.58E-07	2.41E-08	3.19E-06	6.89E-07
			0.7	0.753	0.0052	0.7637	0.0323	9.37E-07	1.81E-08	2.67E-06	1.96E-07
			0.95	0.759	0.0298	0.9415	0.0122	9.90E-07	7.58E-08	3.08E-06	2.08E-07
Distorted (Fig. 1C)	0.1x	0.25	0.05	0.945	0.0244	0.0594	0.0093	1.24E-06	9.60E-07	1.99E-06	8.38E-07
			0.3	0.910	0.0028	0.3261	0.0050	2.57E-07	7.43E-09	2.85E-06	1.56E-08
			0.5	0.917	0.0065	0.5064	0.0132	2.65E-07	1.60E-08	2.90E-06	1.40E-08
			0.7	0.896	0.0060	0.7480	0.0116	1.99E-07	3.24E-08	2.88E-06	7.99E-09
			0.95	1.203	0.0610	0.5256	0.0829	3.48E-06	0.00E+00	2.81E-06	1.51E-08
		1	0.05	0.926	0.0018	0.0212	0.0010	3.04E-07	9.37E-10	9.00E-06	9.20E-07
			0.3	0.922	0.0022	0.2765	0.0103	3.05E-07	7.80E-09	3.15E-06	1.31E-07
			0.5	0.923	0.0010	0.4592	0.0046	3.27E-07	3.19E-09	3.18E-06	4.21E-08
			0.7	0.924	0.0011	0.6618	0.0103	3.62E-07	1.43E-08	3.09E-06	5.17E-08
			0.95	0.924	0.0005	0.9304	0.0140	5.27E-07	9.88E-08	2.94E-06	3.01E-08
		4	0.05	1.065	0.1428	0.3319	0.2774	2.88E-07	1.09E-09	2.03E-07	8.43E-08
			0.3	0.844	0.0108	0.1615	0.0214	2.97E-07	9.70E-10	5.75E-05	1.61E-05
			0.5	0.847	0.0163	0.3647	0.0277	3.02E-07	3.61E-09	7.51E-06	1.72E-06
			0.7	0.894	0.0143	0.6459	0.0249	2.99E-07	4.95E-09	4.03E-06	5.90E-07
			0.95	0.931	0.0091	0.9462	0.0033	3.06E-07	1.53E-08	3.10E-06	1.50E-07
	0.33x	0.25	0.05	0.990	0.0772	0.0990	0.0386	1.18E-06	5.14E-07	1.69E-06	5.00E-07
			0.3	0.723	0.0153	0.7023	0.0339	2.26E-07	4.12E-08	2.63E-06	1.75E-08
			0.5	0.716	0.0048	0.9038	0.0114	6.96E-08	1.81E-08	2.75E-06	7.25E-09
			0.7	0.799	0.0006	0.9310	0.0019	4.28E-08	4.03E-09	2.83E-06	1.33E-08
			0.95	0.903	0.0075	0.9842	0.0158	2.32E-04	1.16E-04	2.88E-06	7.99E-09
		1	0.05	0.922	0.0021	0.0077	0.0018	1.03E-06	1.01E-09	3.48E-08	0.00E+00
			0.3	0.924	0.0003	0.6243	0.1016	1.07E-06	4.58E-07	1.45E-06	3.33E-07
			0.5	0.922	0.0016	0.7318	0.0245	6.96E-07	3.56E-08	2.27E-06	4.94E-08
			0.7	0.922	0.0008	0.8509	0.0333	6.19E-07	9.99E-08	2.51E-06	6.49E-08
			0.95	0.920	0.0001	0.9928	0.0002	6.72E-08	2.39E-09	2.78E-06	2.99E-22
		4	0.05	0.939	0.0097	0.0869	0.0185	9.64E-07	1.54E-09	3.48E-02	0.00E+00
			0.3	0.786	0.0079	0.3650	0.3175	6.73E-07	3.19E-07	3.58E-07	3.23E-07
			0.5	0.687	0.0087	0.6880	0.3116	3.65E-07	3.31E-07	4.33E-04	4.32E-04
			0.7	0.840	0.0251	0.7403	0.2581	4.45E-07	3.43E-07	7.75E-07	3.67E-07
			0.95	0.809	0.0051	0.9794	0.0013	7.02E-07	1.50E-08	2.34E-06	1.88E-08

Key

Diffusion constant difference factor: Ratio of simulated diffusion constants (0.1x: 2.9 x10^{-6} cm^2/ s, 2.9 x 10^{-7} cm^2/s and 0.33x: 2.9 x 10^{-6} cm^2/s, 9.7 x 10^{-7} cm^2/s)

α_S: Relative fluorescent intensity of the slow component

$a_{f,Th}$: Simulated/theoretical mole fraction of the fast component

a_f: Mole fraction of the fast component returned from the analysis

C_T: Total concentration in (molecules/μm^3)

SEM: standard error of the mean for 3 trials

D_S: Diffusion constant of the slow component (cm^2/s)

D_F: Diffusion constant of the fast component (cm^2/s)

Fitting Bound Conditions (Equation 1):

τ_{sf}: 1E-7 ≤ x ≤ 0.1

τ_{ss}:1E-5 <= x <= 0.1

N_f: 0 ≤ x ≤ 1

N_s: 0 ≤ x ≤ 1

REFERENCES

1 Culbertson, M. J.; Williams, J. T. B.; Cheng, W. L.; Stults, D. A.; Wiebracht, E. R.; Kasianowicz, J. J.; Burden, D. L. *Anal. Chem.* **2007**, *79*, 4031.

2 Culbertson, M. J.; Burden, D. L. *Rev. Sci. Instrum.* **2007**, *78*, 044102.